COBEM 2023 27TH INTERNATIONAL CONGRESS OF MECHANICAL ENGINEERING

ABCM Brazilian Society of Mechanical Sciences and Engineering
27th ABCM International Congress of Mechanical Engineering
December 04-08, 2023, Florianópolis-SC, Brazil

COB-2023-0851
TWO-PHASE FRICTIONAL PRESSURE DROP AT HIGH SATURATION TEMPERATURES IN A HORIZONTAL MICRO-SCALE CHANNEL

Daniel Borba Marchetto
Heat Transfer Research Group, São Carlos School of Engineering – University of São Paulo, 13566-590, São Carlos, Brazil
daniel.marchetto@usp.br

Rémi Revellin
Université de Lyon, INSA Lyon, CNRS, CETHIL, UMR5008, 69621, Villeurbanne, France
remi.revellin@insa-lyon.fr

Romuald Rullière
Université de Lyon, INSA Lyon, CNRS, CETHIL, UMR5008, 69621, Villeurbanne, France
romuald.rulliere@insa-lyon.fr

Gherhardt Ribatski
Heat Transfer Research Group, São Carlos School of Engineering – University of São Paulo, 13566-590, São Carlos, Brazil
ribatski@sc.usp.br

Abstract. *In order to meet current and future energy demands, the efficient use of resources, as well as the progressive replacement by renewable alternatives is needed. Therefore, solutions for efficient energy generation and heat exploitation have emerged over the last years. Organic Rankine cycles (ORCs) and high temperature heat pumps (HTHPs), as well as their combination in reversible energy storage systems are promising approaches. The evaporation process in these cycles occurs at high saturation temperatures, leading to intermediate-to-high reduced pressures for most of the employed refrigerants. Thermophysical properties are deeply affected by the reduced pressure increase, resulting in thermohydraulic behaviors different from those typically verified at low temperatures. Despite the growing interest in ORCs and HTHPs, there is a shortage of flow boiling experimental studies at high temperatures, and the literature is even more scarce considering investigations with low-global warming potential (GWP) refrigerants. In this context, the present work presents an evaluation of the two-phase pressure drop for the refrigerants R1233zd(E) and R245fa flowing at saturation temperatures between 75ºC and 95°C inside a horizontal adiabatic stainless-steel tube with an internal diameter of 2 mm. Pressure gradient data are reported for mass velocities varying from 180 to 570 kg/m²s.The effects of the experimental parameters were similar to those reported for data at low pressures, in which the pressure gradient increases with the mass velocity increment and the saturation temperature reduction. The experimental results are compared against 15 prediction methods from literature and the effect of the saturation temperature on their accuracy is evaluated. Reasonable agreement was verified, with five methods predicting more than 80% of the database within error bands of ±30%. However, only six methods presented reduction of the deviations with increasing the saturation temperature, with five of them being based on the homogeneous model.*

Keywords: *two-phase flow, pressure drop, flow boiling, microchannel, organic Rankine cycle*

1. INTRODUCTION

Historically, most of the flow boiling experimental studies using organic refrigerants has been conducted at low saturation temperatures (T_{sat}), focused on HVAC (Heating, ventilating and air-conditioning) systems. However, it can be noticed a currently growing interest in high-temperature applications. One of the main technologies that has been drawing attention is the organic Rankine cycle (ORC), which is pointed out as a promising alternative for obtaining electricity from low-grade heat sources as geothermal, biomass and solar power (Liu *et al*., 2014, Marinheiro *et al*., 2022). According to Zhang *et al*. (2018), typical ORCs heat sources operate at 100-250°C, which results in evaporating temperatures ranging between 50 and 150°C. The high-temperature heat pumps (HTHPs) have also stood out as effective heating and cooling systems, which allow to recover waste heat into hot water or steam. The HTHPs heat source temperatures are higher than 40°C, and can reach 120°C (Arpagaus *et al*., 2018). In addition, Halon *et al*. (2022) pointed out that the rapidly processing speed requirements growth and, consequently, the increase of the quantity of integrated circuits, raised the typical low temperature working environments of electronics cooling (0-85°C) to high-temperature levels (85-500°C or more) that include aerospace, power and automotive industries.

Due to the high evaporation temperatures of the above-mentioned applications, flow boiling at intermediate-to-high reduced pressures (p_r) is verified for most of the organic refrigerants typically employed in these systems. As p_r rises, vapor density (ρ_v) increases, while the liquid density decreases (ρ_l), converging to the same value when the saturation pressure reaches the critical value ($p_r = 1$). In addition, the enthalpy of vaporization (i_{lv}) and the surface tension gradually reduce, while the liquid specific heat ($c_{p,l}$) slightly increases as p_r rises. Non-linear behaviors are also verified for ρ_v, ρ_l, i_{lv} $c_{p,l}$ in the vicinity of the critical point. According to Charnay *et al.* (2014), these changes in the thermophysical properties affect the two-phase flow characteristics, leading to different flow topologies and heat transfer mechanisms, which can impact the reliability of the prediction methods currently available in the literature, since most of them were developed for low p_r.

Despite the growing interest in applications that involve high-temperature evaporation, flow boiling studies at high T_{sat} has not advanced at the same rate. Pressure drop and flow pattern are key parameters in the design of evaporators for thermal systems, however their evaluation at high saturation temperatures were only reported in a few investigations (Zhang and Webb, 2001, Vijayarangan *et al.*, 2007, Charnay *et al.*, 2014, 2015, Layssac *et al.*, 2018). The scenario is even more scarce for low-global warming potential (GWP) refrigerants (Arcasi *et al.*, 2022, Li and Hrnjak, 2022). In this context, the present paper presents an experimental investigation of the two-phase frictional pressure drop and flow patterns of refrigerants R245fa and R1233zd(E) at saturation temperatures between 75 and 95°C. The first refrigerant is frequently pointed out as a high-performance fluid in ORCs (Su *et al.* 2017), and the second is its low- GWP substitute. Experimental results were obtained for a 2 mm inner diameter adiabatic tube for mass velocities (G) ranging from 180 to 570 kg/m²s.

2. EXPERIMENTAL APPARATUS

The experimental facility previously used by Charnay *et al.* (2015) and Layssac *et al.* (2018) for pressure drop and flow pattern investigations was modified in the present study, and it is schematically shown in Fig. 1. The working fluid is driven along a closed loop by an oil-free gear micropump, and its mass flow rate is measured by a Coriolis mass flow meter. A bypass line connects the inlet and outlet of the micropump, and it is used when the mass flow rate reduction is necessary. A filter is installed downstream the micropump in order to remove particles dispersed in the test fluid. A needle microvalve is placed upstream the preheater in order to minimize the propagation of pressure fluctuations associated with thermal instability effects during flow boiling in a small diameter channel (Qu and Mudawar, 2003) and ensure a fine adjustment of the saturation pressure and mass flow rate. The working fluid is heated and evaporated along the preheater, in order to control the vapor quality at the test section inlet. A glass tube is placed downstream the test section to visualize the flow pattern, which is recorded using a high-speed camera (Photron® SA3). K-type thermocouples and absolute pressure sensors (Keller® PA23), installed upstream the preheater and downstream the visualization section, are used to measure the refrigerant temperature and pressure, respectively. The working fluid is condensed and subcooled in a plate heat exchanger by exchanging heat with the auxiliary fluid (Kryo 20). In order to adjust the system pressure, the refrigerant inside the reservoir is heated by the auxiliary fluid. Two thermostatic baths control the temperature of the liquid Kryo 20 flowing in the plate heat exchanger and the refrigerant reservoir. The components of the main loop and the pipelines are insulated from the environment through ceramic fiber covered with elastomeric foam.

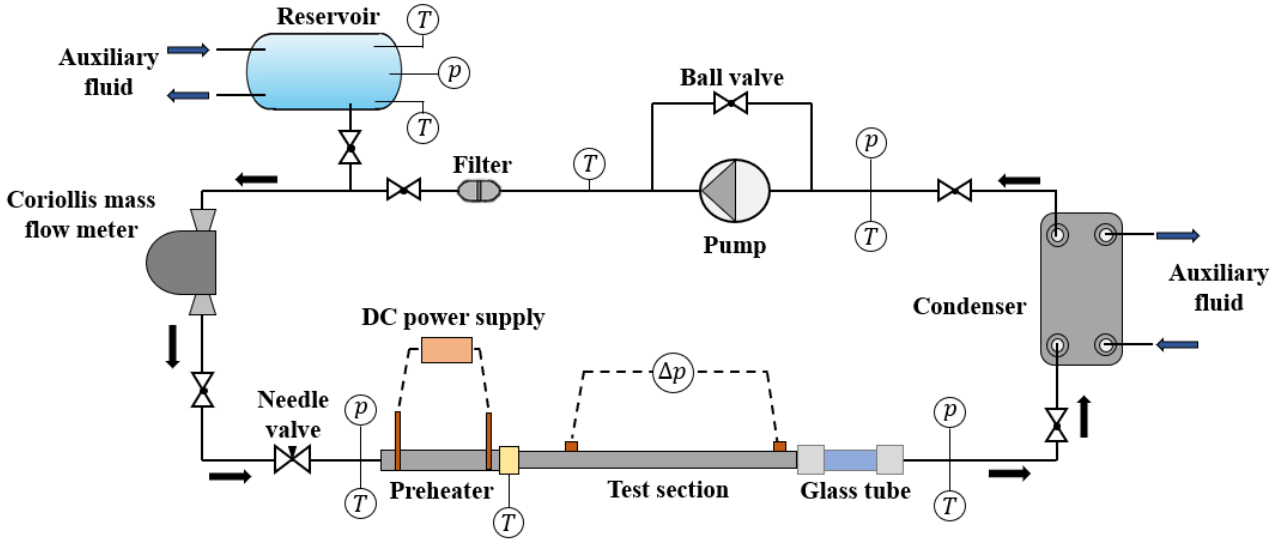

Figure 1. Schematic diagram of the experimental apparatus.

Figure 2 schematically presents the preheating, test and visualization sections. The preheater consists of a spirally-shaped stainless-steel tube with inner and outer diameters of 4 and 6 mm, respectively. The heating effect along the preheater is achieved through Joule effect by directly powering the surface of the tube using copper electrodes positioned 1910 mm apart, which are connected to a DC power supply. The test section is a straight stainless-steel tube with an outer diameter of 6 mm, in which two pressure taps are welded 300 mm apart from each other. The inner diameter of the test tube was measured through confocal microscopy, and the average value obtained was 2.07 mm. The visualization section is a 200 mm long Pyrex tube, with inner and outer diameters of 2 and 6 mm, respectively.

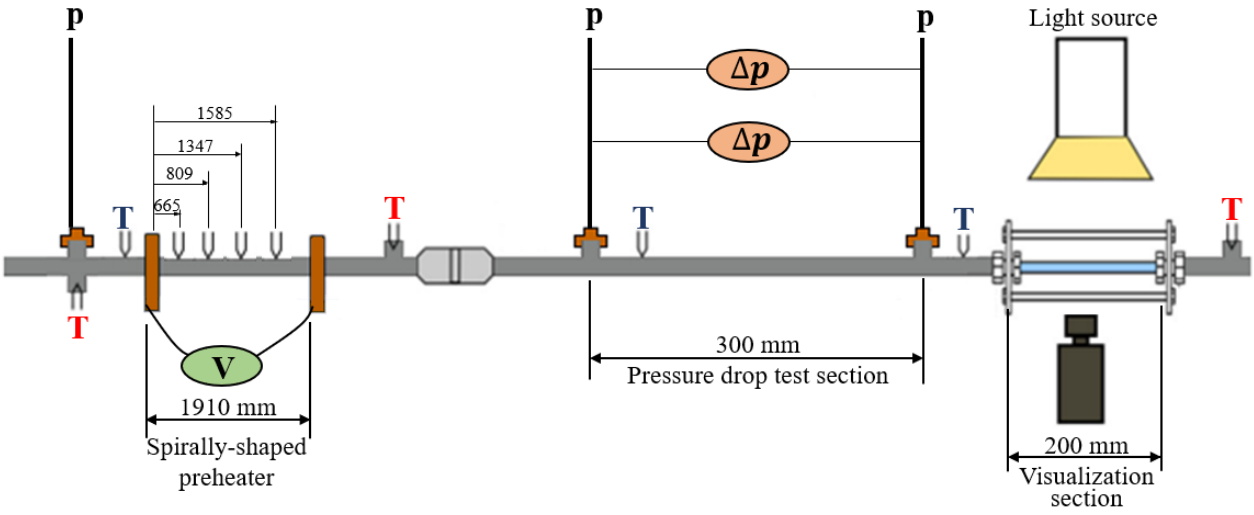

Figure 2. Detailed view of the preheating, test and visualization sections.

The pressure drop is measured by two differential pressure sensors (Endress Hauser® Rosemount 3051) with measuring ranges of 0-50 mbar and 0-2 bar, which are connected to the pressure taps, as depicted in Fig. 2. Four K-type thermocouples are positioned at the outer surface of the preheater, 665, 809, 1347 and 1585 mm apart from the copper electrode. K-type thermocouples and absolute pressure sensors are used to measure the temperature of the working fluid at the inlet and outlet of each subsection depicted in Fig. 2.

3. DATA TREATMENT PROCEDURE AND VALIDATION

The average saturation temperature of the working fluid is based on the average pressure along the test section, which is given as follow:

$$\bar{p}_{sat} = \frac{p_{in,TS} + (p_{in,TS} + \Delta p_{measured})}{2} \tag{1}$$

where $p_{in,TS}$ is the pressure measured by the absolute pressure sensor placed upstream the test section and $\Delta p_{measured}$ is the pressure drop measured by the differential sensor.

The mass velocity is given by the following relation:

$$G = \frac{4.\dot{m}}{\pi D_i^2} \tag{2}$$

where $\dot{m}$ is the mass flow rate measured by the Coriolis mass flow meter and D_i is the internal diameter of the test section.

The vapor quality at test section inlet is given as follows:

$$x_{in,TS} = \frac{i_{in,TS} - i_l(p_{in,TS})}{i_v(p_{in,TS}) - i_l(p_{in,TS})} \tag{3}$$

where $i_l(p_{in,TS})$ and $i_v(p_{in,TS})$ are the liquid and vapor phase specific enthalpies of the working fluid evaluated at the pressure at the inlet of the test section ($p_{in,TS}$).

The specific enthalpy of the working fluid at the test section inlet is estimated by an energy balance along the preheater, as follows:

$$i_{in,TS} = i_{in,PH} + \frac{\dot{Q}_{eff,PH}}{\dot{m}} \tag{4}$$

where $\dot{Q}_{eff,PH}$ is the preheater effective heating power and $i_{in,PH}$ is the liquid saturated specific enthalpy corresponding to the temperature measured at the preheater inlet.

The effective preheater heating power, $\dot{Q}_{eff,PH}$, is given as the electrical power delivered by the power supply, ($\dot{Q}_{el} = I.U$) minus the heat losses to the environment ($\dot{Q}_{loss}$):

$$\dot{Q}_{eff,PH} = I.U - \dot{Q}_{loss,PH} = \left(1 - \eta_{loss,PH}\right).I.U \tag{5}$$

where I is the electrical current delivered by the DC power supply, U is the corresponding voltage measured along the preheater, and $\eta_{loss,PH}$ is the relative heat losses.

The relative heat losses were estimated during single-phase flow experiments, comparing the electrical power delivered by the DC source with the enthalpy variation along the preheater, as described in the following relation:

$$\eta_{loss,PH} = \frac{I.U - \dot{m}.c_{p,l}(T_{out} - T_{in})}{I.U} \tag{6}$$

where T_{in} and T_{out} are the temperatures of the working fluid at the preheater inlet and outlet, respectively.

Single-phase experimental results were obtained at different mass velocities, and it was verified the reduction of $\eta_{loss,PH}$ with increasing G, which is associated with the increase of the heat transfer coefficient (HTC) along the preheater and, consequently, the overall thermal resistance reduction. The heat transfer coefficient was calculated at the wall temperature measurement positions indicated in Fig. 2 through the Newton's colling law, and the relative heat losses were correlated as functions of the average HTC ($\bar{h}$) according to a power law, $\eta_{loss,PH} = a.\bar{h}^{b}$. Figure 3 presents the experimental results obtained and the corresponding curve fits for both refrigerants, determined through the least squares method. The fitted correlations were used to estimate the relative heat losses during two-phase flow experiments.

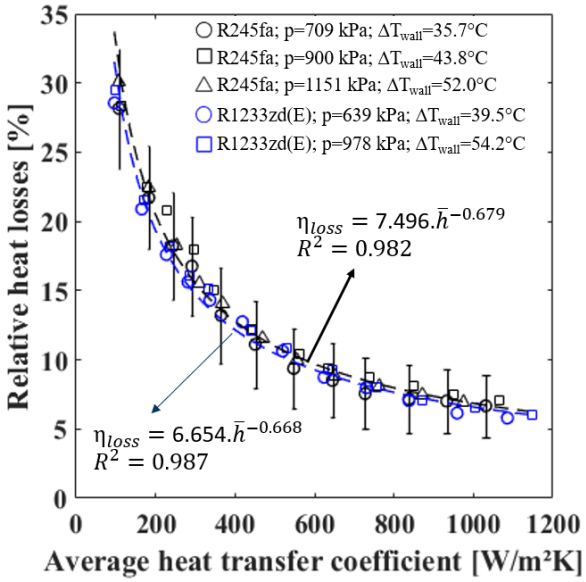

Figure 3. Effect of the average heat transfer coefficient on the preheater relative heat losses.

The frictional pressure gradient is given by the following relation:

$$\left(\frac{dp}{dz}\right)_f = \frac{\Delta p_f}{L} \tag{7}$$

where Δp_f is the frictional component of the pressure drop and L is the distance between the pressure taps in which the pressure sensors are connected.

In the present investigation, experiments were conducted during adiabatic flow conditions, which, in general, lead to a negligible accelerational component of the pressure drop. In order to confirm this hypothesis, the correlation developed by Revellin *et al*. (2012) was used to predict the vapor quality increment due to the flashing effect, which remained lower than 0.006. As a consequence, the accelerational pressure drop associated with the flashing effect was always lower than

2% of the measured pressure drop, which is close to its average uncertainty of 2.1%. Therefore, in the present study, it was assumed that Δp_f is equal to the pressure drop measured by the differential sensors ($\Delta p_{measured}$).

The validation of the experimental apparatus was also performed during single-phase flow experiments, comparing the measured pressure drop with the corresponding predictions according to Blasius correlation. Figure 4 presents the comparison between the Fanning friction factor calculated from the experimental data and the predictions based on Blasius correlation ($f = 0.079Re^{-0.25}$). A reasonable agreement is verified between experimental and predicted values, with all data predicted within an error margin lower than ±14%, and a mean absolute error (MAE) of only 10.4%.

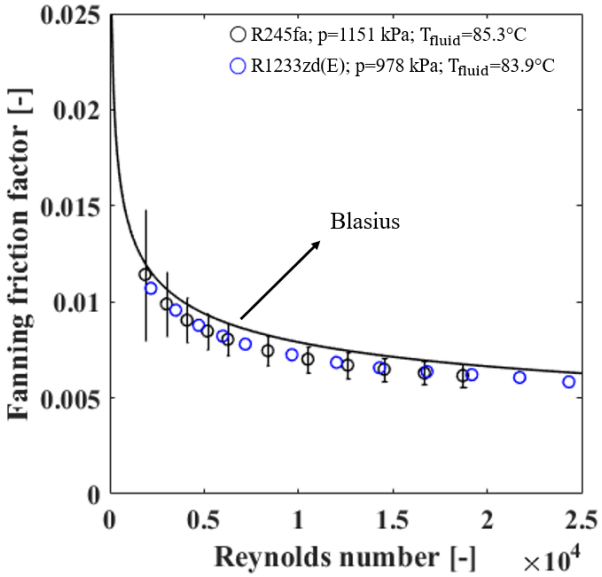

Figure 4. Comparison between experimental Fanning friction factor and Blasius correlation.

The experimental apparatus described in section 2 is monitored and controlled using a personal computer with a Labview (National Instruments®) interface. The K-type thermocouples are connected to a cold junction compensation system, which contains a platinum Pt100 used as temperature reference. A calibration process was performed for temperatures between 25 and 115°C prior to experiments, using a model 9142 Fluke® calibration device. The average uncertainty of the temperatures measured by the thermocouples was 0.15°C, which was calculated according to the procedure proposed by Abernethy and Thompson Jr. (1973). For the remaining sensors and measuring devices, the uncertainties were assumed equal to the specifications provided by the manufactures. The method of sequential perturbation (Moffat, 1998) was used to estimate the uncertainties of the calculated parameters. As a result, the mass velocity, saturation temperature, vapor quality and frictional pressure gradient average uncertainties were 4.6%, 0.22°C, 0.025 and 2.1%, respectively.

4. RESULTS

4.1 Flow patterns

In the present study, two main flow patterns were identified: intermittent and annular. Figure 4 presents the evolution of the flow patterns verified for $G = 560$ kg/m²s and $T_{sat} = 95$°C with increasing vapor quality. It is important to remark that at low vapor qualities, plug flow pattern is verified (Fig. 4a), while with a slight increment of *x*, slug flow was typically verified (Fig. 4b), however, for simplicity, both flow patterns were classified as intermittent. In addition, at vapor qualities close to 1, the liquid film is almost imperceptible (Fig. 4e), but is not possible to guarantee the occurrence of dryout or mist flow, since the last thermocouple attached to the preheater surface was placed relatively far from its outlet (325 mm) making it impossible to identify the sharp increase of the surface temperature. Therefore, the dryout and mist flow patterns were not differentiated from annular in the present study.

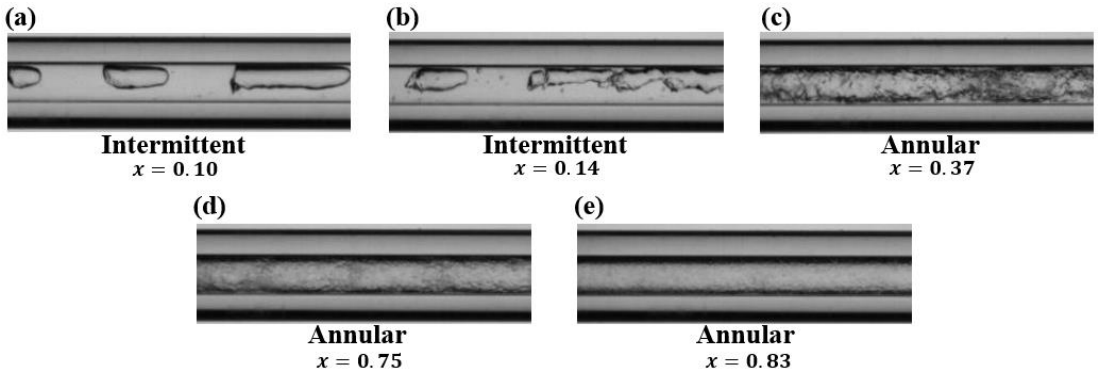

Figure 4. Flow pattern evolution for T_{sat}=*95*°C and *G=560* kg/m²s.

Figure 5 presents the mass velocity effect on the intermittent-annular transition at two different saturation temperatures. As well as reported at low T_{sat} studies (Revellin *et al*., 2006, Ong and Thome, 2011), the mass velocity increment anticipates this flow pattern transition. Comparing Figs. 5a and 5b, it is verified that increasing T_{sat} postpones the intermittent-annular transition. Figure 5 also presents the lines corresponding to the transition criteria proposed by Ong and Thome (2011). At T_{sat}=75°C the prediction method of Ong and Thome (2011) seems to be more accurate in predicting the intermittent-annular transition for high mass velocities, however, at T_{sat}=95°C, a better agreement is verified for mass velocities of 187 and 280 kg/m²s.

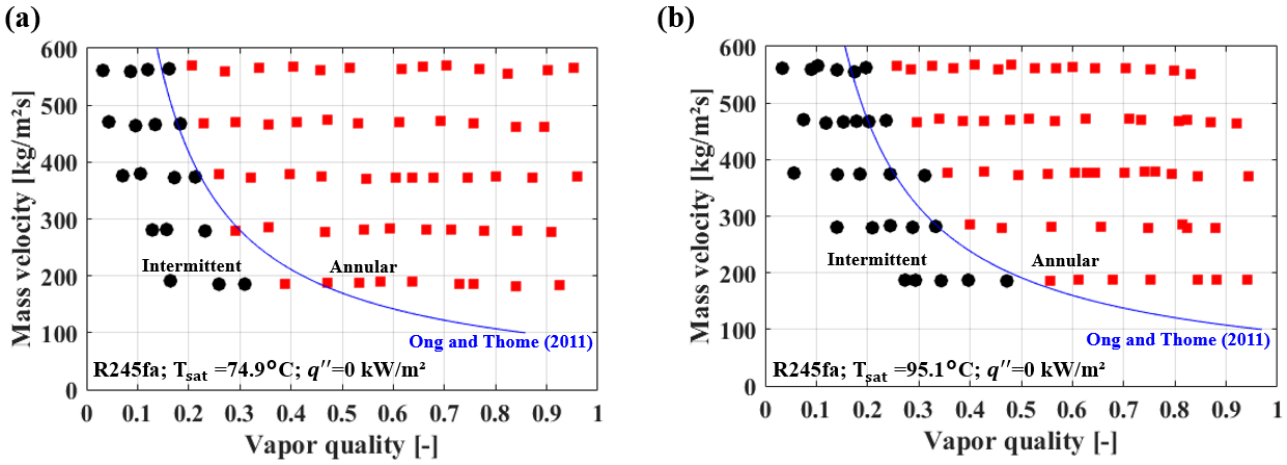

Figure 5. Mass velocity effect on the intermittent-annular transition at (a) T_{sat}=*75*°C and (b) T_{sat}=*95*°C.

4.2 Pressure drop

Figure 6 presents the mass velocity effect on the frictional pressure gradient. At both 75 and 95°C saturation temperatures, the *G* increment increases the pressure gradient, which is associated with the flow velocity increment and, consequently, the increment of shear stress at the liquid-vapor interface and between liquid and tube surface. The experimental results also indicate that the mass velocity increase seems to anticipate the pressure gradient peak, which might be associated with the higher amount of entrainment at higher *G*, anticipating the damping of disturbance waves at the liquid-vapor interface (Morse *et al*., 2021).

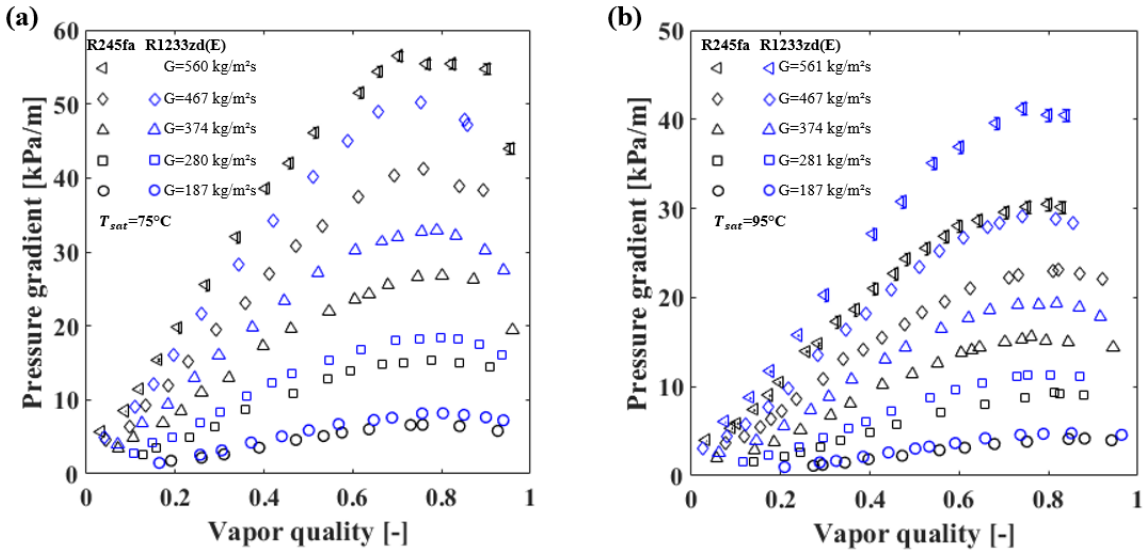

Figure 6. Mass velocity effect on the frictional pressure gradient for (a) T_{sat}=*75*°C and (b) T_{sat}=*95*°C.

Figure 7 presents the effect of the saturation temperature on the frictional pressure gradient. The increment of the saturation temperature increases the vapor phase density, which reduces the two-phase flow velocity and, consequently, the frictional pressure gradient. The approximation of liquid and vapor densities at higher saturation temperatures also accounts for the reduction of the pressure gradient, since the difference between the velocities of the phases is reduced, decreasing the interfacial shear. Table 1 presents the thermophysical properties of both working fluids at the saturation temperatures evaluated in the present study.

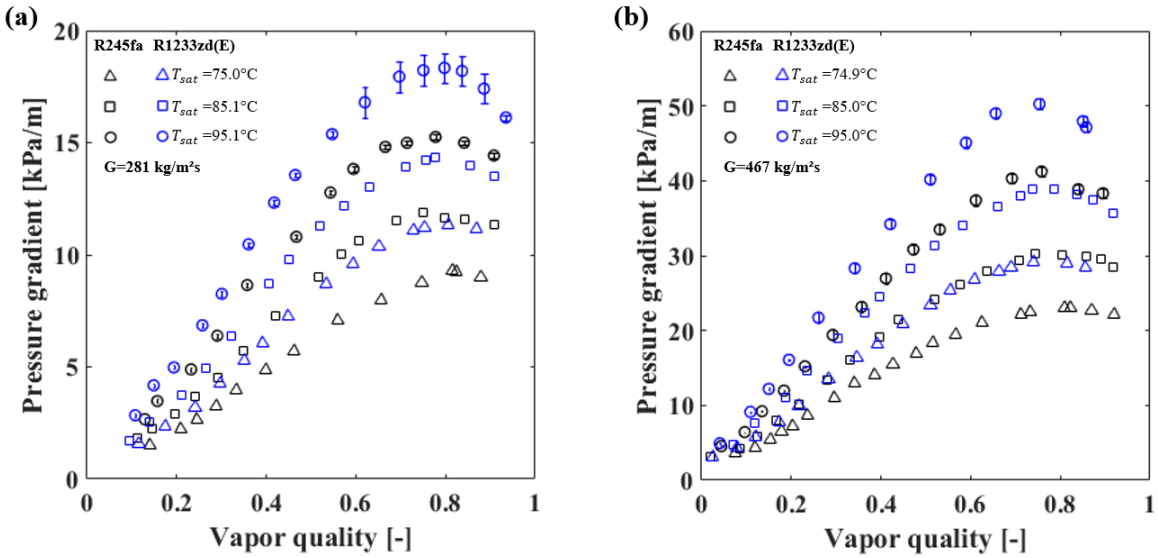

Figure 7. Saturation temperature effect on the frictional pressure gradient for (a) G=*281* kg/m²s and (b) G=*467* kg/m²s.

Table 1. Properties of the fluids evaluated in the present study (Lemmon *et al.*, 2018).

Property	**75°C**		**95°C**	
	R245fa	**R1233zd(E)**	**R245fa**	**R1233zd(E)**
p_r **[-]**	0.190	0.160	0.309	0.258
μ_l **[Pa.s]**	0.000214	0.000177	0.000166	0.000144
μ_v **[Pa.s]**	$1.23.10^{-5}$	$1.21.10^{-5}$	$1.31.10^{-5}$	$1.28.10^{-5}$
μ_l/μ_v **[-]**	17.40	14.63	12.67	11.25
ρ_l **[Pa.s]**	1187.9	1129.9	1114.2	1066.9
ρ_v **[Pa.s]**	38.295	30.692	63.898	50.004
ρ_l/ρ_v **[-]**	31.02	36.81	17.44	21.34

Figures 6 and 7 also indicate that the frictional pressure gradients for the R1233zd(E) are higher than those for the R245fa at all evaluated T_{sat} and G. At the same saturation temperature, the reduced pressure of the first refrigerant is lower than that of the second, so, reduced vapor phase densities are verified for the R1233zd(E). In addition, the liquid-vapor densities ratio is 19-22% higher for the R1233zd(E), justifying the higher pressure gradients verified for this refrigerant.

The 450 adiabatic frictional pressure gradient datapoints obtained in the present study were compared against 15 prediction methods from literature. Table 3 presents the statistical results of the comparisons in means of the MAE and the percentage of data predicted within an error band of $\pm$30% ($\lambda_{30\%}$). The empirical correlation proposed by Müller-Steinhagen and Heck (1986) presented the lowest MAE, 14.8%, and predicted the largest parcel of the database within error bands of $\pm$ 30%, 93.1%. Curiously, this method did not consider experimental results at high saturation temperatures in the adjust of its empirical constants and exponents.

Reasonably accuracies were also achieved by the methods of Cicchitti *et al.* (1962), Zhang and Webb (2001), Sempértegui-Tapia and Ribatski (2017) and Kim and Mudawar (2013). The first three methods did not present relevant variations of the MAEs with increasing the saturation temperature, while the MAE of the method proposed by Kim and Mudawar (2013) raised more than 7% when T_{sat} increased from 75°C to 95°C. Considering the 15 methods evaluated, only 6 of them presented higher accuracy at T_{sat}=*95*°C than in 75°C, with five of them been based on the homogeneous model. No slip ratio is the hypothesis adopted by the homogeneous model, so, as the difference between the liquid and vapor phase velocities decreases with increasing T_{sat}, it is expected that the accuracy of the homogeneous-based methods improves at higher saturation temperatures.

Table 2. Statistical analysis results of the comparison between pressure drop database and prediction methods.

Method		**All data**	**75°C**	**95°C**
Homogeneous-based methods				
McAdams (1942)	**MAE [%]**	34.1	36.5	31.9
	$\lambda_{30\%}$ [%]	33.6	25.5	40.1
Cicchitti *et al.* (1962)	**MAE [%]**	19.2	18.1	19.5
	$\lambda_{30\%}$ [%]	92.0	93.6	93.0
Dukler *et al*. (1964)	**MAE [%]**	36.6	40.1	33.7
	$\lambda_{30\%}$ [%]	27.1	18.4	35.0
Beattie and Whalley (1982)	**MAE [%]**	29.7	32.0	27.3
	$\lambda_{30\%}$ [%]	42.0	38.3	45.9
Lin *et al*. (1991)	**MAE [%]**	38.7	32.8	29.3
	$\lambda_{30\%}$ [%]	31.1	35.5	42.7
Garcia *et al.* (2003)	**MAE [%]**	35.3	39.7	31.4
	$\lambda_{30\%}$ [%]	30.0	20.6	38.8
Two-phase multiplier-based methods				
Lockhart and Martinelli (1949)	**MAE [%]**	93.7	65.7	124.0
	$\lambda_{30\%}$ [%]	30.4	41.1	19.7
Chisholm (1973)	**MAE [%]**	69.5	64.1	75.9
	$\lambda_{30\%}$ [%]	36.7	38.3	32.5
Friedel (1979)	**MAE [%]**	23.6	18.0	27.8
	$\lambda_{30\%}$ [%]	71.8	81.6	65.0
Mishima and Hibiki (1996)	**MAE [%]**	31.2	21.2	41.4
	$\lambda_{30\%}$ [%]	68.2	83.0	54.1
Zhang and Webb (2001)	**MAE [%]**	15.4	15.1	15.1
	$\lambda_{30\%}$ [%]	89.1	87.2	91.7
Kim and Mudawar (2013)	**MAE [%]**	16.7	13.1	20.3
	$\lambda_{30\%}$ [%]	84.9	92.2	79.6
Empirical correlations				
Müller-Steinhagen and Heck (1986)	**MAE [%]**	14.8	15.2	14.0
	$\lambda_{30\%}$ [%]	93.1	94.3	91.7
Xu and Fang (2012)	**MAE [%]**	22.0	18.8	24.2
	$\lambda_{30\%}$ [%]	72.9	77.3	70.1
Sempértegui-Tapia and Ribatski (2017)	**MAE [%]**	18.9	17.7	19.5
	$\lambda_{30\%}$ [%]	84.0	88.6	82.2

5. CONCLUSIONS

The pressure drop experimental results obtained in the present study at high saturation temperatures presented similar behavior to those previously reported in low-temperature studies, i.e. increase of the frictional pressure gradient with increasing the mass velocity and reducing the saturation temperature. Among the 15 prediction methods evaluated, 5 of them were able to predict more than 80% of the database raised in the present study with absolute deviations lower than 30%. Some empirical correlations and two-phase multiplier prediction methods presented strong loss of accuracy with increasing the saturation temperature, while 5 of the 6 homogeneous-based methods evaluated provided more accurate predictions at high temperatures. In addition, flow-pattern image analysis indicated that stratification effects are verified despite the small diameter of the test tube and lower liquid-vapor density differences. The postponement of the intermittent-annular transition to higher vapor qualities was verified with reducing mass velocity and increasing saturation temperature.

6. ACKNOWLEDGEMENTS

The authors gratefully acknowledge the São Paulo Research Foundation (FAPESP, Brazil) for the scholarships given to the first author, under Contract Numbers 2019/22105-5 and 2020/06705-0. The authors also acknowledge the support through the Thematic Grant provided by FAPESP under Contract Number 2016/09509-01.

7. REFERENCES

Abernethy, R. B., Thompson Jr. J. W., 1973, Uncertainty in gas turbine measurements. In 9th Propulsion conference, pp. 1230.

Arcasi, A., Mastrullo, R., Mauro, W. A., Viscito, L., 2022, Adiabatic frictional pressure gradient during flow boiling of pure refrigerant R1233zd and non-azeotropic mixtures R448A, R452A and R455A, Journal of Physics: Conference Series, 2177, pp. 012045.

Arpagaus, C., Bless, F., Uhlmann, M., Schiffmann, J., Bertsch, S. S., 2018, High temperature heat pumps: Market overview, state of the art, research status, refrigerants, and application potentials, Energy, Vol. 152, pp. 985-1010.

Beattie, D. R. H., Whalley, P. B., 1982, A simple two-phase frictional pressure drop calculation method, International Journal of Multiphase Flow, Vol. 8, pp. 83-87.

Charnay, R., Bonjour, J., Revellin, R., 2014, Experimental investigation of R-245fa flow boiling in minichannels at high saturation temperatures: Flow patterns and flow pattern maps, International Journal of Heat and Fluid Flow, Vol. 46, pp. 1-16.

Charnay, R., Revellin, R., Bonjour, J., 2015, Discussion on the validity of prediction tools for two-phase flow pressure drops from experimental data obtained at high saturation temperatures. International Journal of Refrigeration, Vol. 54, pp. 98-125.

Chisholm, D., 1973, Pressure gradients due to friction during the flow of evaporating two-phase mixtures in smooth tubes and channels, International Journal of Heat and Mass Transfer, Vol. 16, pp. 347-358.

Cicchitti, A. Lombardi, C. Silvestri, M. Soldaini, G., Zavattarelli, R., 1962, Two-phase cooling experiments—pressure drop, heat transfer and burnout measurements, Energia Nucleare, Vol. 7, pp. 407–425.

Dukler, A. E., Wicks III, M., Cleveland, R. G., 1964, Frictional pressure drop in two-phase flow: B. An approach through similarity analysis, AIChE Journal, pp. 44-51.

Friedel, L., 1979, Improved friction pressure drop correlation for horizontal and vertical two-phase pipe flow. Proc. of European Two-Phase Flow Group Meet., Ispra, Italy.

Garcıa, F., Garcıa, R., Padrino, J. C., Mata, C., Trallero, J. L., Joseph, D. D., 2003, Power law and composite power law friction factor correlations for laminar and turbulent gas–liquid flow in horizontal pipelines. International Journal of Multiphase Flow, Vol. 29, pp. 1605-1624.

Halon, S, Krolicki, Z, Revellin, R, Zajaczkowski, B., 2022, Heat transfer characteristics of flow boiling in a micro channel array with various inlet geometries, International Journal of Heat and Mass Transfer, Vol. 187, pp. 122549.

Kim, S. M., Mudawar, I., 2013, Universal approach to predicting two-phase frictional pressure drop for mini/micro-channel saturated flow boiling, International Journal of Heat and Mass Transfer, Vol. 58, pp.718-734.

Layssac, T., Lips, S., Revellin, R., 2018, Experimental study of flow boiling in an inclined mini-channel: Effect of inclination on flow pattern transitions and pressure drops, Experimental Thermal and Fluid Science, Vol. 98, pp. 621-633.

Lemmon, E.W., Bell, I.H., Huber, M.L., McLinden, M.O., 2018, NIST Standard Reference Database 23: Reference Fluid Thermodynamic and Transport Properties-REFPROP, Version 10.0, National Institute of Standards and Technology, Standard Reference Data Program, Gaithersburg.

Li, H., Hrnjak, P., 2022, Heat transfer coefficient, pressure gradient, and flow patterns of R1233zd(E) and R1336mzz(Z) evaporating in a microchannel tube, International Journal of Heat and Mass Transfer, Vol. 182, pp. 121992.

Lin, S., Kwok, C. C. K., Li, R. Y., Chen, Z. H., Chen, Z. Y., 1991, Local frictional pressure drop during vaporization of R-12 through capillary tubes, International Journal of Multiphase Flow, Vol. 17, pp. 95-102.

Liu, W., Meinel, D., Wieland, C., Spliethoff H., 2014, Investigation of hydrofluoroolefins as potential working fluids in organic Rankine cycle for geothermal power generation, Energy, Vol. 67, pp. 106-116.

Lockhart, R. W., Martinelli, R. C., 1949, Proposed correlation of data for isothermal two-phase, two component flow in pipes, Chemical Engineering Progress, Vol. 45, pp. 39-48.

Marinheiro, M. M., Coraça, G. M., Cabezas-Gomez, L., Ribatski, G., 2022. Detailed transient assessment of a small-scale concentrated solar power plant based on the organic Rankine cycle, Applied Thermal Engineering, Vol. 204, pp. 117959.

McAdams, W., Woods, W., Bryan, R., 1942, Vaporization inside horizontal tubes II: Benzene-oil mixtures, Trans. ASME, Vol. 64, pp. 193-200.

Mishima, K., Hibiki, T., 1996, Some characteristics of air-water two-phase flow in small diameter vertical tubes. International journal of multiphase flow, Vol. 22, pp. 703-712.

Moffat, R. J., 1988, Describing the uncertainties in experimental results, Experimental Thermal and Fluid Science, Vol. 1, pp. 3-17.

Morse, R. W., Moreira, T. A., Chan, J., Dressler, K. M., Ribatski, G., Hurlburt, E. T., McCarroll, L. L., Nellis, G. F., Berson, A., 2021. Critical heat flux and the dryout of liquid film in vertical two-phase annular flow, International Journal of Heat and Mass Transfer, Vol. 177, pp. 121487.

Müller-Steinhagen, H., Heck, K., 1986, A simple friction pressure drop correlation for two-phase flow in pipes, Chemical Engineering and Processing: Process Intensification, Vol. 20, pp. 297-308.

Ong, C. L., Thome, J. R., 2011, Macro-to-microchannel transition in two-phase flow: Part 1 – Two-phase flow patterns and film thickness measurements, Experimental Thermal and Fluid Science, Vol. 35, pp. 37-47.

Qu, W., Mudawar, I., 2003, Measurement and prediction of pressure drop in two-phase micro-channel heat sinks, International Journal of Heat and Mass Transfer, Vol. 46, pp. 2737-2753.

Revellin, R., Dupont, V., Ursenbacher, T., Thome, J. R., Zun, I., 2006, Characterization of diabatic two-phase flows in microchannels: Flow parameter results for R-134a in a 0.5 mm channel, International Journal of Multiphase Flow, Vol. 32, pp. 755-774.

Revellin, R., Lips, S., Neveu, P., Bonjour, J., 2012, A comprehensive non-equilibrium thermodynamic analysis applied to a vapor–liquid two-phase flow of a pure fluid, International Journal of Multiphase Flow, Vol. 42, pp. 184-193.

Sempértegui-Tapia, D. F., Ribatski, G., 2017, Two-phase frictional pressure drop in horizontal micro-scale channels: experimental data analysis and prediction method development. international journal of refrigeration, Vol. 79, pp. 143-163.

Su, W., Zhao, L., Deng, S., 2017, Simultaneous working fluids design and cycle optimization for Organic Rankine cycle using group contribution model, Applied Energy, Vol. 202, pp. 618-627.

Vijayarangan, B. R., Jayanti, S., Balakrishnan, A. R., 2007, Pressure drop studies on two-phase flow in a uniformly heated vertical tube at pressures up to the critical point, International Journal of Heat and Mass Transfer, Vol. 50, pp. 1879-1891.

Xu, Y., Fang, X., 2012, A new correlation of two-phase frictional pressure drop for evaporating flow in pipes, International Journal of Refrigeration, Vol. 35, pp. 2039-2050.

Zhang, M., Webb, R. L., 2001, Correlation of two-phase friction for refrigerants in small-diameter tubes, Experimental Thermal and Fluid Science, Vol. 25, pp. 131-139.

Zhang, Y., Tian, R., Dai, X., Wang, D., Ma, Y., Li, H., Shi, L., 2018, Experimental study of R134a flow boiling in a horizontal tube for evaporator design under typical Organic Rankine Cycle pressures, International Journal of Heat and Fluid Flow, Vol. 71, pp.210–219.

8. RESPONSIBILITY NOTICE

The authors are the only responsible for the printed material included in this paper.